machines

MDPI

Article

Neural Network Based Adaptive Event-Triggered Control for Quadrotor Unmanned Aircraft Robotics

Pukun Lu [1,2], Meng Liu [1,2], Xiuyu Zhang [1,2,*], Guoqiang Zhu [1,2,*], Zhi Li [3] and Chun-Yi Su [4]

[1] School of Automation Engineering, Northeast Electric Power University, Jilin 132012, China; 2202000551@neepu.edu.cn (P.L.); 1202200013@neepu.edu.cn (M.L.)
[2] Jilin Provincial International Joint Research Center of Precision Drive and Intelligent Control, Northeast Electric Power University, Jilin 132012, China
[3] State Key Laboratory of Synthetical Automation for Process Industries, Northeastern University, Shenyang 110819, China; lizhi1@mail.neu.edu.cn
[4] Department of Mechanical and Industrial Engineering, Concordia University, Montreal, QC H3B 1R6, Canada; cysu@alcor.concordia.ca
* Correspondence: zhangxiuyu@neepu.edu.cn (X.Z.); zhugq@neepu.edu.cn (G.Z.)

Abstract: With the aim of addressing the problem of the trajectory tracking control of quadrotor unmanned aircraft robots (UARs), in this study, we developed a neural network and event-triggering mechanism-based adaptive control scheme for a quadrotor UAR control system. The main technologies included this scheme are as follows. (1) Under the condition that only the quadrotor's position information can be obtained, a modified high-gain state observer-based adaptive dynamic surface control (DSC) method was applied and the tracking control of quadrotor UARs was acquired. (2) An event-triggered mechanism for UARs was designed, in which the energy consumption was greatly reduced and the communication efficiency between the system and the control terminal was improved. (3) By selecting appropriate parameters, appropriate initial conditions for the adaptive laws, and establishing a high-gain state observer, a tracking performance of L_∞ could be achieved. Finally, simulation results of the hardware-in-loop strategy are presented. The control method we propose here outperformed the traditional backstepping sliding mode control (BSMC) scheme.

Keywords: quadrotor control system; dynamic surface control; event-triggered

Citation: Lu, P.; Liu, M.; Zhang, X.; Zhu, G.; Li, Z.; Su, C.-Y. Neural Network Based Adaptive Event-Triggered Control for Quadrotor Unmanned Aircraft Robotics. *Machines* **2022**, *10*, 617. https://doi.org/10.3390/machines10080617

Academic Editor: Raffaele Di Gregorio

Received: 22 June 2022
Accepted: 23 July 2022
Published: 27 July 2022

1. Introduction

The problem of controlling quadrotor systems has recently attracted significant attention. It has been commonly applied in the fields of rescue missions and agricultural service; however, a problem continues to disrupt the control of quadrotor systems [1–4]. Because of factors including measurement errors, quadrotor unmanned aircraft robots (UARs) are modeled as complex nonlinear systems, which increases the difficulty involved in controlling these systems [5–8]. Therefore, the question of how to choose a reasonable and effective adaptive algorithm for the accurate control of quadrotor UARs has become an urgent problem.

In practical applications, external disturbances are always ignored in the process of controller design, which results in lower system robustness. Thus, the design of the controller is the key to obtaining a good performance in trajectory tracking under the influence of external disturbances. In [9,10], a proportional-integral-derivative (PID) controller provided active interference suppression by combining active disturbance rejection technology with the PID control method to ensure the rapid observation of errors. In [11], the uncertainty and the model's measurement noise were generated by means of a neural network approximator. A robust compensator was proposed to eliminate any approximation errors and achieve effective high-precision trajectory tracking control. In [12–15], to improve the control precision of a quadrotor system, an algorithm based on the BSMC approachwas proposed, which overcame the nonlinear effects of the quadrotor.

However, another problem remains, in that a "differential explosion" can occur when the design of the controller steps relies on the BSMC control scheme.To deal with the differential explosion problems, refs. [16,17] combined the extended state observer and the dynamic surface schemes to propose a control method for quadrotor trajectory tracking, which ensured the stability of the control system and effectively solved the differential explosion problem. In [18], a dynamic model of quadrotor flight height was established. Ref. [18] achieved this by comparing the traditional first-order SMC algorithm with the second-order SMC algorithm to obtain a new quadrotor height control algorithm. However, the proposals introduced thus far involve strong assumptions and require all states of the quadrotor to be available.

In addition, the process of signal transmission also has an important role in the quadcopter control system. In [19], to cope with the high-pressure problem of constant signal transmissions from the quadcopter and the console, a control scheme based on a fixed-time-triggered mechanism was introduced into the steps of controller design, which relieved the communication pressure by using periodic transmissions to update the control signals. However, when the control performance is unsatisfactory, a method used to improve the control performance is to reduce the sampling period. At present, if the control signal is still updated at the previous frequency, this inevitably leads to unwanted resource waves [20]. In [21,22], control schemes based on an event-triggered mechanism were applied to cope with the fixed-time triggering approach, which showed good performance.

The previous trigger moment influences the event-triggered mechanism and determines the next trigger moment. At the time of triggering,the console and the quadrotor do not need to communicate; therefore, the communication pressure of the quadrotor can be decreased. However, the event triggering mechanism may suffer from Zeno behavior, in which the trigger event can be triggered numerous times in a narrow timeframe [23–25]. In relation to this issue, the basic properties of the minimum event-triggered intervals in event-triggered mechanisms were studied in [26]. In [27–30], the event-triggered mechanism was introduced into the design of the controller, which greatly reduced the transmission pressure of the control signal. Therefore, a feasible method involves adding an event-triggered mechanism into the process of controller design for quadrotors in order to decrease the pressure of quadrotor communication. The application of event triggering mechanisms has been examined in several studies with respect to the controller design process for quadrotor UARs. However, the authors mentioned above, such as [22], have not considered the problem of quadrotor position tracking control when a quadrotor UAR can only measure its position in relation to certain pieces of information.

In summary, many algorithms have been developed to solve control problems related to quadrotor UARs. However, according to our recent search results, coping with the control problems of quadrotor UARs remains a challenging issue. To solve these problems, based on [12,13,20,31], a neural network and event-triggering-mechanism-based adaptive control method for a quadrotor UAR control system is proposed in this paper. An unknown air drag coefficient, aerodynamic drag coefficient, and rotational inertia are approximated by means of a neural network. The trajectory tracking control of a quadrotor UAR's positioning is achieved by means of the DSC technique and a controller design involving state feedback. The trajectory tracking control of a quadrotor UAR's attitudeis addressed by means of an output feedback controller. The main innovations of this paper are:

(1) To our best knowledge, for the first time we present an adaptive DSC scheme with a modified high-gain observer that has been designed for quadrotor UARs under the condition that only the position data of the quadrotor system are available, along with the testing of the quadrotor UAR controller in the hardware-in-loop simulation platform. Thus, the underactuation problem in quadrotor UARs is perfectly solved, and precise tracking performance is obtained.
(2) By designing an event triggering mechanism for quadrotor UARs, the control signal can be updated immediately when threshold conditions are triggered. Therefore, compared with the time-triggered control mechanism, the energy consumption can be

greatly reduced, and the communication pressure between the system and the control terminal is lowered using the event triggering mechanism.

(3) By setting the original conditions of the high-gain state observer, adaptive control laws, and the appropriate controller parameters, a tracking performance of L_∞ for underactuated quadrotor UARs is achieved.

2. Problem Statement

2.1. Model Construction

The quadrotor body coordinate system and ground coordinate system are shown in Figure 1, wherein the quadrotor has a total of six degrees of freedom in the output, with translational degrees of freedom in three directions and rotational degrees of freedom in three directions. Moreover, the thrust of the UARs is produced by four motors, which located at the corners of the quadrotor body. Among these, F_2 and F_4 are driven by two positive propeller motors, and F_1 and F_3 are driven by two anti-positive propeller motors. However, this structure leads to the need for the balancing of yaw torque as required. For example, under the condition in which the lift force is greater than the quadrotor's mass, the quadrotor will rise vertically when increasing the output power of the four motors at the same time. Moreover, if $F_2 > F_4$, $F_1 = F_3$, a pitching motion will be observed and the machine will exhibit translational motion along the y-axis. Hence, by adjusting the speed of the motors, attitude control and position control of the UAR can be attained.

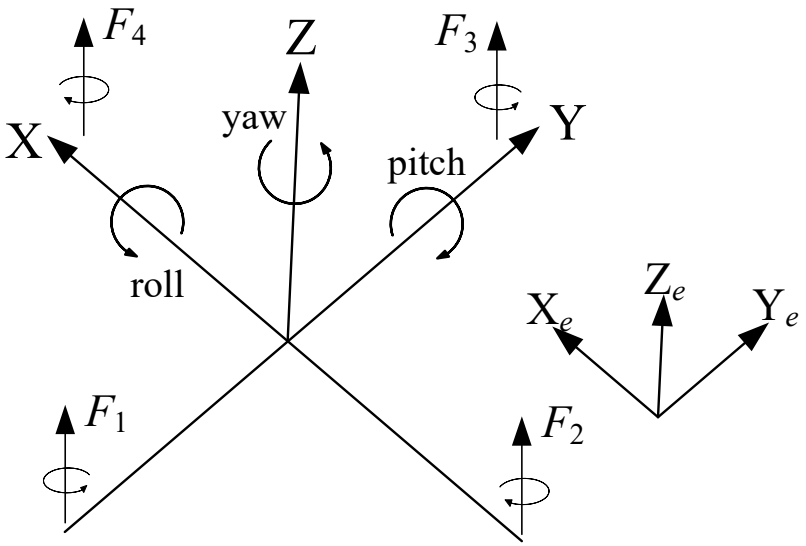

Figure 1. Quadrotor body coordinate system and ground coordinate system.

Faced with the control problem of quadrotor UARs, here the rigid body transdynamics, as well as the Newton–Euler equations are used to model the quadrotor. We have $[\phi, \theta, \psi] \in \mathbb{R}^3$ and $[p, q, r] \in \mathbb{R}^3$, with ϕ, θ, ψ designating the roll, pitch and yaw angles with regard to the ground coordinates, which are represented by $Ox_e y_e z_e$, and p, q, r are the angular speed the of roll, pitch, and yaw movements with respect to the body coordinates, which are denoted by $Ox_b y_b z_b$. An explanation of the other symbols is given in Table 1. To clarify the connections among the inertial coordinate system and the body coordinate system, we use conversion equations. Choosing the x-axis as an example [32]

$$\begin{aligned} X &= x, \\ Y &= \cos\phi y - \sin\phi z, \\ Z &= \sin\phi y + \cos\phi z, \end{aligned} \tag{1}$$

where X, Y, Z are the inertial coordinate system and x, y, z are the quadrotor body coordinate system. The transformation matrix can be expressed as

$$R(x,\phi) = \begin{bmatrix} 1 & 0 & 0 \\ 0 & \cos\phi & -\sin\phi \\ 0 & \sin\phi & \cos\phi \end{bmatrix} \tag{2}$$

Table 1. The notation for the quadrotor.

Symbol	Nomenclature
$F_i, i = 1,2,3,4$	Lift force
K_X, K_Y, K_Z	Unknown coefficients of air resistance
m	Mass of quadrotor
g	Acceleration of gravity
$\bar{\omega}$	Relative speed of the cross-coupled rotor
I_x, I_y, I_z	Rotary inertia for all axis
I_r	Moment of inertia for all motors
d_ϕ, d_θ, d_ψ	Coefficient of unknown aerodynamic drag
l	Distance from the center to the rotor
$\tau_i, i = 1,2,3,4$	Torque
$d_X(t), d_Y(t), d_Z(t), d_1(t), d_2(t), d_3(t)$	Bounded external disturbances

The rotation matrix of the Y axis and the Z axis can be obtained as follows:

$$R(y,\theta) = \begin{bmatrix} \cos\theta & 0 & \sin\theta \\ 0 & 1 & 0 \\ -\sin\theta & 0 & \cos\theta \end{bmatrix} \tag{3}$$

$$R(z,\psi) = \begin{bmatrix} \cos\psi & -\sin\psi & 0 \\ \sin\psi & \cos\psi & 0 \\ 0 & 0 & 1 \end{bmatrix} \tag{4}$$

Then the overall conversion relationship between the inertial coordinate system and the body coordinate system is:

$$R(\phi,\theta,\psi) = \begin{bmatrix} \cos\theta\cos\psi & A & C \\ \cos\theta\sin\psi & B & D \\ -\sin\theta & \cos\theta\sin\phi & \cos\phi\cos\theta \end{bmatrix} \tag{5}$$

with $A = \cos\psi\sin\phi\sin\theta - \cos\phi\sin\psi$, $B = \cos\phi\cos\psi + \sin\phi\sin\theta\sin\psi$, $C = \sin\phi\sin\psi + \sin\phi\cos\psi\sin\theta$, $D = \cos\phi\sin\theta sin\psi - cos\psi sin\phi$. $F_E = F_1 + F_2 + F_3 + F_4$. Then, the motion model, as well as the angular motion of the quadrotor with respect to the ground coordinate system, can be expressed as:

$$\begin{aligned}
\ddot{X} &= \left[F_E(\sin\phi\sin\psi + \cos\phi\cos\psi sin\theta) - K_X\dot{X}\right]/m + d_X(t) \\
\ddot{Y} &= \left[F_E(\cos\psi\sin\theta\sin\psi - \cos\psi sin\phi) - K_Y\dot{Y}\right]/m + d_Y(t) \\
\ddot{Z} &= \left[F_E(\cos\phi\cos\theta) - K_Z\dot{Z} - mg\right]/m + d_Z(t) \\
\ddot{\phi} &= \left[\dot{\theta}\dot{\psi}(I_y - I_z) - I_r\dot{\theta}\bar{\omega} - d_\phi\dot{\phi} + l(F_4 - F_2)\right]/I_x + d_1(t) \\
\ddot{\theta} &= \left[\dot{\phi}\dot{\psi}(I_z - I_x) - I_r\dot{\theta}\bar{\omega} - d_\theta\dot{\theta} + l(F_3 - F_1)\right]/I_y + d_2(t) \\
\ddot{\psi} &= \left[\dot{\phi}\dot{\theta}(I_x - I_y) - d_\psi\dot{\psi} + (\tau_2 + \tau_4 - \tau_1 - \tau_3)\right]/I_z + d_3(t)
\end{aligned} \tag{6}$$

with $\bar{\omega} = \omega_2 + \omega_4 - \omega_1 - \omega_3$. We can determine that $x_{X,1} = X$, $x_{X,2} = \dot{X}$, $x_{Y,1} = Y$, $x_{Y,2} = \dot{Y}$, $x_{Z,1} = Z$, $x_{Z,2} = \dot{Z}$, $x_1 = \phi$, $x_2 = \dot{\phi}$, $x_3 = \theta$, $x_4 = \dot{\theta}$, $x_5 = \psi$, $x_6 = \dot{\psi}$. Then, Equation (6) can be rewritten as follows

$$\begin{cases} \dot{x}_{X,1} = x_{X,2}, \\ \dot{x}_{X,2} = (\cos x_1 \sin x_3 \cos x_5 + \sin x_1 \sin x_5)U_4 - a_1 x_{X,2} + d_X(t), \\ \dot{x}_{Y,1} = x_{Y,2}, \\ \dot{x}_{Y,2} = (\cos x_1 \sin x_3 \sin x_5 - \sin x_1 \cos x_5)U_4 - a_2 x_{Y,2} + d_Y(t), \\ \dot{x}_{Z,1} = x_{Z,2}, \\ \dot{x}_{Z,2} = (\cos x_1 \cos x_3)U_4 - a_3 x_{Z,2} + d_Z(t) - g, \\ y_i = x_{i,1}, i = X, Y, Z, \\ \dot{x}_1 = x_2, \\ \dot{x}_2 = a_4 x_4 x_6 + a_5 \bar{\omega} x_4 - a_6 x_2 + U_1 + d_1(t), \\ \dot{x}_3 = x_4, \\ \dot{x}_4 = a_7 x_2 x_6 + a_8 \bar{\omega} x_2 - a_9 x_4 + U_2 + d_2(t), \\ \dot{x}_5 = x_6, \\ \dot{x}_6 = a_{10} x_2 x_4 - a_{11} x_6 + U_3 + d_3(t), \\ y_j = x_{2*j-1}, j = 1, 2, 3, \end{cases} \tag{7}$$

with $a_1 = K_X/m$, $a_2 = K_Y/m$, $a_3 = K_Z/m$, $a_4 = \left(I_y - I_z\right)/I_x$, $a_5 = I_r/I_x$, $a_6 = d_\phi/I_x$, $a_7 = (I_z - I_x)/I_y$, $a_8 = I_r/I_y$, $a_9 = d_\theta/I_y$, $a_{10} = \left(I_x - I_y\right)/I_z$, $a_{11} = d_\psi/I_z$ are unknown; U_1, U_2, U_3 and U_4 are the control inputs, wherein $U_1 = l(F_4 - F_2)/I_x$, $U_2 = l(F_3 - F_1)/I_y$, $U_3 = (\tau_2 + \tau_4 - \tau_1 - \tau_3)/I_z$, $U_4 = (F_1 + F_2 + F_3 + F_4)/m$.

Remark 1. *It should be noted that the bounded external disturbances $d_X(t)$, $d_Y(t)$, $d_Z(t)$, $d_1(t)$, $d_2(t)$, and $d_3(t)$ considered in this paper could denote the force of the wind, wind gusts, noise, electromagnetism, and bad weather while the quadrotor system is working.*

2.2. Radial Basis Function Neural Networks (RBFNNs)

In this work, under Lemma 1, any continuous function on the compact sets can be approximated by applying the RBFNNs.

Lemma 1 (see [33]). *With $f_i(\xi_i) : \Omega_{\xi_i} \to \mathbb{R}, i = X, Y, Z$, are smooth and $\Omega_{\xi_i} \subset \mathbb{R}^q$ being compact sets, ξ_i represents the RBFNN's input, and q is the input dimension for any $\varepsilon_m > 0$, by properly selecting η_i and $\xi_k \in \mathbb{R}^q, k = 1, \ldots, N$, then, for some sufficiently large integer N, an RBFNN is factored in and expressed as:*

$$\begin{aligned} f_i(\xi_i) &= \psi_i^T(\xi_i)\vartheta_i^* + \varepsilon_i, i = X, Y, Z \\ &\forall \xi_i \in \Omega_{\xi_i} \subset \mathbb{R}^q, |\varepsilon_i| \le \varepsilon_m \end{aligned} \tag{8}$$

where $Y_i(\xi_i)$ is the output of the RBFNN, and ϑ_i^* denotes the optimal weight vector of ϑ_i and is expressed as $\vartheta_i^* = \arg\min_{\vartheta_i \in R^N} \left\{ \sup_{\xi_i \in \Omega_{\xi_i}} |Y_i(\xi_i) - f_i(\xi_i)| \right\}$, $\psi_k(\xi) = \exp\left(-\frac{\|\xi - \xi_k\|}{2\eta^2}\right)$. This is the basis function, where $\eta > 0$ serves as the width of the basis function and $\xi_k \in R^q$ is the center of the basis function, which serves as a constant vector, with ε_i representing the approximated errors, with $\varepsilon_i = f_i(\xi_i) - \vartheta_i^{*T}\psi_i(\xi_i)$.

For proof, let

$$\begin{aligned} U_X &= (\cos x_1 \sin x_3 \cos x_5 + \sin x_1 \sin x_5)U_4 \\ U_Y &= (\cos x_1 \sin x_3 \sin x_5 - \sin x_1 \cos x_5)U_4 \\ U_Z &= (\cos x_1 \cos x_3)U_4, \end{aligned} \tag{9}$$

and $f_X(x) = -a_1 x_{X,2}$, $f_Y(x) = -a_2 x_{Y,2}$, $f_Z(x) = -a_3 x_{Z,2}$. Therefore, (7) can be expressed as

$$\begin{cases} \dot{x}_{X,1} = x_{X,2}, \\ \dot{x}_{X,2} = U_X + f_X(x) + d_X(t), \\ \dot{x}_{Y,1} = x_{Y,2}, \\ \dot{x}_{Y,2} = U_Y + f_Y(x) + d_Y(t), \\ \dot{x}_{Z,1} = x_{Z,2}, \\ \dot{x}_{Z,2} = U_Z + f_Z(x) + d_Z(t) - g, \\ y_i = x_{i,1}, i = X, Y, Z, \\ \dot{x}_1 = x_2, \\ \dot{x}_2 = a_4 x_4 x_6 + a_5 \bar{\omega} x_4 - a_6 x_{Z,2} + U_1 + d_1(t), \\ \dot{x}_3 = x_4, \\ \dot{x}_4 = a_7 x_2 x_6 + a_8 \bar{\omega} x_2 - a_9 x_4 + U_2 + d_2(t), \\ \dot{x}_5 = x_6, \\ \dot{x}_6 = a_{10} x_2 x_4 - a_{11} x_6 + U_3 + d_3(t), \\ y_j = x_{2*j-1}, j = 1, 2, 3. \end{cases} \tag{10}$$

Note that the air drag coefficients are K_X, K_Y, K_Z, whereas the continuous functions represented by system parameters a_1, a_2, and a_3 are also unknown. Thus, the above proof can be approximated by means of RBFNNs in Lemma 1.

To define x_{5r}, it is important to define the desired trajectories of the yaw angle. The next step is to realize the control scheme. To achieve this, the following assumptions are required [34]:

A1: The reference trajectories are $y_{ri}, i = X, Y, Z$, and x_{5r} are the smooth and bounded functions, $[y_{ri}, \dot{y}_{ri}, \ddot{y}_{ri}]^T$, which are part of a set of known compact , Ω_r when $t > 0$.

A2: The external disturbances can be represented as $d_i(t) \leq \bar{d}_i$, wherein $\bar{d}_i$ are positive constants, $i = 1, 2, 3, X, Y, Z$.

A3: The angles of roll and pitch are limited to $(-\pi/2, \pi/2)$ in accordance with the physical meaning. In particular, the yaw angle range of $(-\pi/2, \pi/2)$ was selected for the purposes of this study.

3. Proposed Methodology

In this paper, we present a neural network and event-triggered-mechanism-based adaptive control method. The architecture of the control method is presented in Figure 2. The output-feedback controller is designed to achieve the position model part from the quadrotor. The part of the model related to the attitude of the quadrotor can be realized using the state-feedback method.

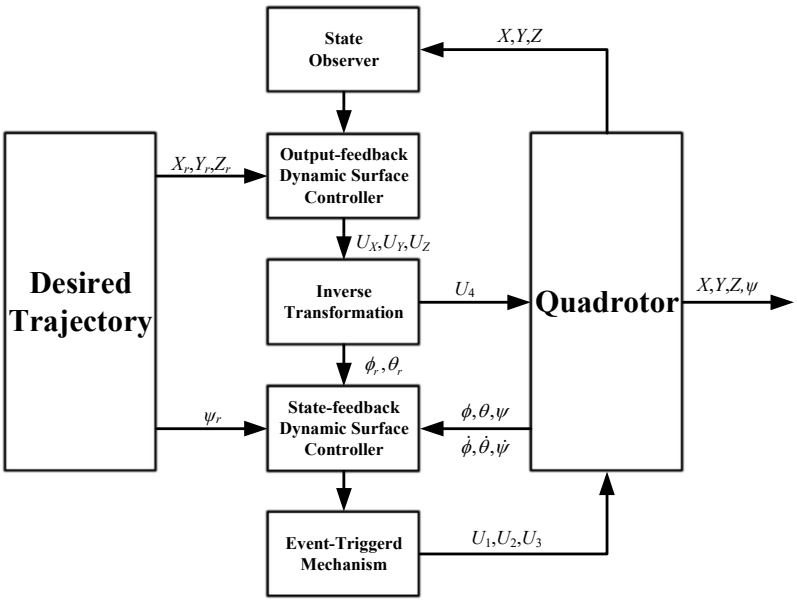

Figure 2. The architecture of the proposed control method.

3.1. Controller Design for Positioning Trajectory Tracking

The position model of the quadrotor is expressed as follows:

$$\begin{aligned} \dot{x}_i &= A_i x_i + \Psi_i^T(\xi_i)\vartheta_i^* + \varepsilon_i + D_{ib}(t) + G_i + b_i U_i \\ y_i &= x_{i,1} \end{aligned} \tag{11}$$

with $A_i = \begin{bmatrix} 0 & 1 \\ 0 & 0 \end{bmatrix}$, $\vartheta_i^* = \begin{bmatrix} 0 \\ \vartheta_{i,2}^* \end{bmatrix}$, $b_i = \begin{bmatrix} 0 \\ 1 \end{bmatrix}$, $\Psi_i^T = \begin{bmatrix} 0 & 0 \\ 0 & \psi_{i,2} \end{bmatrix}$, $\varepsilon_i = \begin{bmatrix} 0 \\ \varepsilon_{i,2} \end{bmatrix}$, $G_X = G_Y = \begin{bmatrix} 0 \\ 0 \end{bmatrix}$, $G_Z = \begin{bmatrix} 0 \\ -g \end{bmatrix}$, $D_{ib}(t) = \begin{bmatrix} 0 \\ d_i(t) \end{bmatrix}$, $i = X, Y, Z$. Let $B_i = \varepsilon_i + D_{ib}(t) + G_i$, and $A_{i,0} = A_i - q_i e_{i,1}^T = \begin{bmatrix} -q_{i,1} & 1 \\ -q_{i,2} & 0 \end{bmatrix}$, where $q_i = \begin{bmatrix} q_{i,1} \\ q_{i,2} \end{bmatrix}$, and $A_{i,0}$ denotes a Hurwitz matrix determined by selecting the proper vector q_i. It follows that

$$\begin{aligned} \dot{x}_i &= A_{i,0} x_i + q_i y_i + \Psi_i^T(\xi_i)\vartheta_i^* + B_i + b_i U_{i,0} \\ y_i &= e_1^T x_i, i = X, Y, Z. \end{aligned} \tag{12}$$

Inspired by [4,35–37] the high-gain K-filter observer is used to estimate the unmeasured states, and the K-filter observer is designed by:

$$\begin{aligned} \dot{v}_{i,0} &= k_i A_{i,0} v_{i,0} + \Delta_i^{-1} e_{i,2} U_{i,0} \\ \dot{\varsigma}_{i,0} &= k_i A_{i,0} \varsigma_{i,0} + k_i q_i y_i \\ \dot{\Xi}_i &= k_i A_{i,0} \Xi_i + \Delta_i^{-1} \Psi_i^T, \end{aligned} \tag{13}$$

where $i = X, Y, Z$, $k_i \geq 1$ denote the positive design parameters, and $e_{i,2}$ is the second coordinate vector in $\mathbb{R}^2$ with

$$\Delta_i = diag\{1, k_i\}. \tag{14}$$

From (13) and (14), the estimated state vector is used as follows:

$$\hat{x}_i = \Delta_i \varsigma_{i,0} + \Delta_i v_{i,0} + \Delta_i \Xi_i \vartheta_i^*. \tag{15}$$

Then, for the estimation error we can obtain:

$$\epsilon_i = x_i - \hat{x}_i, \tag{16}$$

with:

$$\dot{\epsilon}_i = \dot{x}_i - \dot{\hat{x}}_i = A_i \epsilon_i - k_i \Delta_i q_i \epsilon_{i,1} + B_i \tag{17}$$

where $\epsilon_{i,1}$ is the first entries of ϵ_i. Since ϑ_i^* is unknown, the actual states can be estimated with the estimated value $\hat{\vartheta}_i$ of ϑ_i^*, and it follows that:

$$\hat{\dot{x}}_i = \Delta_i \varsigma_{i,0} + \Delta_i v_{i,0} + \Delta_i \Xi_i \hat{\vartheta}_i. \tag{18}$$

Lemma 2. *The quadratic function can be described by:*

$$V_{\epsilon_i} := \epsilon_i^T P_i \epsilon_i \tag{19}$$

with $P_i = \left(\Delta_i^{-1}\right)^T \bar{P}_i \Delta_i^{-1}$, *wherein* $\bar{P}_i = \bar{P}_i^T > 0$ *is a positive definite metrix, which satisfies*

$$A_{i,0}^T \bar{P}_i + \bar{P}_i^T A_{i,0} = -2I, \tag{20}$$

For $k_i \geq 1$, it follows that:

$$\dot{V}_{\epsilon_i} \leq -\frac{k_i}{\lambda_{\max}(\bar{P}_i)} V_{\epsilon_i} + k_i \left(\frac{\|\bar{P}_i\| \|B_i\|_{\max}}{k_i^2}\right)^2. \tag{21}$$

Proof. Please see the proof of Lemma 2 in Appendix A. □

Design of Controller with Dynamic Surface Control Method

Step 1: The error from the first surface can be expressed as

$$S_{i,1} = y_i - y_{ri}. \tag{22}$$

Then, $\dot{S}_{i,1}$ is defined as

$$\dot{S}_{i,1} = \dot{y}_i - \dot{y}_{ri} = x_{i,2} - \dot{y}_{ri}. \tag{23}$$

From (16), we have:

$$\begin{aligned} x_{i,2} &= \hat{x}_{i,2} + \epsilon_{i,2} \\ &= k_i \varsigma_{i,(0,2)} + k_i v_{i,(0,2)} + k_i \Xi_{i,(2)} \vartheta_i^* + \epsilon_{i,2} \end{aligned} \tag{24}$$

where $\Xi_{i,(2)}$ denotes the second row of Ξ_i. Furthermore, we have

$$\begin{aligned} \dot{S}_{i,1} &= k_i \varsigma_{i,(0,2)} + k_i v_{i,(0,2)} + k_i \Xi_{i,(2)} \vartheta_i^* + \epsilon_{i,2} - \dot{y}_{ri} \\ &= k_i \varsigma_{i,(0,2)} + k_i \left(v_{i,(0,2)} - \bar{v}_{i,(0,2)}\right) + k_i \bar{v}_{i,(0,2)} + k_i \Xi_{i,(2)} \vartheta_i^* + \epsilon_{i,2} - \dot{y}_{ri} \end{aligned} \tag{25}$$

where $\bar{v}_{i,(0,2)}$ denote the signals of virtual control. It follows that

$$\bar{v}_{i,(0,2)} = \left(-l_{i,1} S_{i,1} - k_i \varsigma_{i,(0,2)} - \hat{\vartheta}_i^T k_i \Xi_{i,(2)}^T + \dot{y}_{ri}\right)/k \tag{26}$$

where $l_{i,1}$ are design constants and $\hat{\vartheta}_i$ is the estimated values of ϑ_i^*.

$\hat{\vartheta}_i$ denotes the update law, which is expressed as

$$\dot{\hat{\vartheta}}_i = \gamma_{\vartheta_i} \left[k_i \Xi_{i,(2)}^T S_{i,1} - \sigma_{\vartheta_i} \hat{\vartheta}_i\right]. \tag{27}$$

Let $\bar{v}_{i,(0,2)}$ be expressed as the first-order low-pass filter input; it follows that:

$$z_{i,2} + \tau_{i,2} \dot{z}_{i,2} = \bar{v}_{i,(0,2)}, z_{i,2}(0) = \bar{v}_{i,(0,2)}(0) \tag{28}$$

Step 2: Let $S_{i,2}$ be expressed as

$$S_{i,2} = v_{i,(0,2)} - z_{i,2}. \tag{29}$$

Then, $\dot{S}_{i,2}$ is defined as

$$\dot{S}_{i,2} = -k_i q_{i,2} v_{i,(0,1)} + k_i^{-1} U_{i,0} - \dot{z}_{i,2}. \tag{30}$$

The final control law is obtained as

$$U_{i,0} = k_i \left(k_i q_{i,2} v_{i,(0,1)} - l_{i,2} S_{i,2} + \dot{z}_{i,n}\right). \tag{31}$$

Then, the event-triggered-mechanism-based adaptive controller can be expressed as

$$\breve{U}_i(t) = U_{i,0} - g_{i,1} \tanh\left(\frac{k^{-1} S_{i,2} g_{i,1}}{\rho_i}\right), \tag{32}$$

The trigger events are expressed as:

$$\begin{aligned} U_i(t) &= \breve{U}_i(t_n), \forall t \in [t_n, t_{n+1}), \\ t_{n+1} &= \inf\{t > t_n || e_i(t)| \geq g_i\}, \end{aligned} \tag{33}$$

where $t_n, n \in \mathbb{Z}^+, \rho_i > 0, g_{i,1} > g_i$ denote the designed parameters, which are positive, and $e_i(t) = \breve{U}_i(t) - U_i(t)$ represent the errors of measurement. When the trigger events occur, then the control signals $U_i(t)$ are updated to $\breve{U}_i(t_{n+1})$ and the control signals $U_i(t) = \breve{U}_i(t_n)$ are satisfied when $t \in [t_n, t_{n+1})$.

According to (9), it can be seen that U_X, U_Y, U_Z denote the designed control signals. However, there are four variables in (9) , which are given as x_1, x_3, x_5 and U_4, respectively. These four unknown variables must be calculated. However, it is commonly known that the above unknown variables can not be solved by means of three equations. For this reason, an extra signal must be provided in the control scheme. In this paper, the yaw angle, which is represented by x_{5r}, is given and the designed control signal U_3 guarantees that the state x_5 will converge to the reference x_{5r}. Then, reference signals x_{1r}, x_{3r} of x_1, x_3 and U_4 can be obtained by solving Equation (9) as follows: $x_{3r} = \arctan((U_X \cos x_{5r} + U_Y \sin x_{5r})/U_Z), x_{1r} = \arctan((U_X \sin x_{5r} - U_Y \cos x_{5r}) \cos x_{3r}/U_Z), U_4 = U_Z/(\cos x_{1r} \cos x_{3r})$.

3.2. Controller Design of Attitude Trajectory Tracking

The mathematical model of the quadrotor's attitude can be rewritten as:

$$\begin{cases} \dot{x}_{2*j-1} = x_{2*j} \\ \dot{x}_{2*j} = \Theta_{\alpha_j}^T \Gamma_{\alpha_j} + U_{j,0} + d_j(t) \\ y_j = x_{2*j-1} \end{cases} \tag{34}$$

where $j = 1, 2, 3$, $\Theta_{\alpha_1} = [a_4, a_5, a_6]^T$, $\Theta_{\alpha_2} = [a_7, a_8, a_9]^T$, $\Theta_{\alpha_3} = [a_{10}, a_{11}]^T$, $\Gamma_{\alpha_1} = [x_4 x_6, -\varpi x_4, -x_2]^T, \Gamma_{\alpha_2} = [x_2 x_6, \varpi x_2, -x_4]^T, \Gamma_{\alpha_3} = [x_2 x_4, -x_6]^T$.

Step 1: Define the error of the first surface as:

$$S_{2*j-1} = x_{2*j-1} - x_{(2*j-1)r}. \tag{35}$$

For analysis, let Lyapunov functions be defined as:

$$V_{2*j-1} = \frac{1}{2} S_{2*j-1}^2. \tag{36}$$

Then, the time derivatives of $\dot{V}_{2*j-1}$ yield

$$\begin{aligned} \dot{V}_{2*j-1} &= S_{2*j-1} \dot{S}_{2*j-1} \\ &= S_{2*j-1} \left(x_{2*j} - x_{(2*j)d} \right) + S_{2*j-1} x_{(2*j)d} - S_{2*j-1} \dot{x}_{(2*j-1)r}. \end{aligned} \tag{37}$$

Based on the virtual control law $x_{(2*j)d}$, it follows that:

$$x_{(2*j)d} = -k_{2*j-1} S_{2*j-1} + \dot{x}_{(2*j-1)r}. \tag{38}$$

We define z_{2*j}, which can be acquiredby a first-order low-pass filter. It follows that

$$z_{2*j} + \iota_{2*j} \dot{z}_{2*j} = x_{(2*j)d}, z_{2*j}(0) = x_{(2*j)d}(0) \tag{39}$$

where $x_{(2*j)d}$ and ι_{2*j} represent the input as well as the positive time constants of the first-order low-pass filter, respectively. We have

$$\dot{V}_{2*j-1} = S_{2*j-1}(S_{2*j} - k_{2*j-1} S_{2*j-1}) + S_{2*j-1} y_{2*j}. \tag{40}$$

Step 2: Define S_{2*j} as

$$S_{2*j} = x_{2*j} - z_{2*j}. \tag{41}$$

Then, the time derivatives of S_{2*j} yield

$$\begin{aligned} \dot{S}_{2*j} &= \dot{x}_{2*j} - \dot{z}_{2*j} \\ &= \Theta_{\alpha_j}^T \Gamma_{\alpha_j} + U_{j,0} + d_j(t) - \dot{z}_{2*j}. \end{aligned} \tag{42}$$

Define the following Lyapunov functions as:

$$V_{2*j} = \frac{1}{2} S_{2*j}^2 + \frac{1}{2 r_{\Theta_{\alpha_j}}} \tilde{\Theta}_{\alpha_j}^2. \tag{43}$$

Then, we have:

$$\begin{aligned} \dot{V}_{2*j} &= S_{2*j} \dot{S}_{2*j} + \frac{1}{r_{\Theta_{\alpha_j}}} \tilde{\Theta}_{\alpha_j}^T \dot{\hat{\Theta}}_{\alpha_j} \\ &= S_{2*j} (\Theta_{\alpha_j}^T \Gamma_{\alpha_j} + U_{j,0} + d_j(t) - \dot{z}_{2*j}) + \frac{1}{r_{\Theta_{\alpha_j}}} \tilde{\Theta}_{\alpha_j}^T \dot{\hat{\Theta}}_{\alpha_j}. \end{aligned} \tag{44}$$

Therein, the final control law can be obtained as follows:

$$U_{j,0} = -k_{2*j} S_{2*j} - S_{2*j} - \hat{\Theta}_{\alpha_j}^T \Gamma_{\alpha_j} + \dot{z}_{2*j} \tag{45}$$

where $\hat{\vartheta}_{\alpha_j}$ are updated by:

$$\dot{\hat{\Theta}}_{\alpha_j} = r_{\Theta_{\alpha_j}} \left(\Gamma_{\alpha_j} S_{2*j} - \sigma_{\Theta_{\alpha_j}} \hat{\Theta}_{\alpha_j} \right). \tag{46}$$

Then, the event-triggering-mechanism-based adaptive controller can be expressed as

$$\breve{U}_j(t) = (1 + \delta_j) \left[U_{j,0} - \bar{\psi}_j \tanh \left(\frac{S_2 \bar{\psi}_j}{\beta_j} \right) \right], \tag{47}$$

and the trigger events are designed as follows:

$$\begin{aligned} U_j(t) &= \breve{U}_j(t_k), \forall t \in [t_k, t_{k+1}), \\ t_{k+1} &= \inf \left\{ t > t_k \middle| \left| e_j'(t) \right| \geq \delta_j U_j(t) + \psi_j \right\}, \end{aligned} \tag{48}$$

where $t_k, k \in \mathbb{Z}^+, \beta_j > 0, 0 < \delta_j < 1, \psi_j > 0, \bar{\psi}_j \geq \psi_j / (1 - \delta_j)$ are the positive design parameters and $e_j'(t) = \breve{U}_j(t) - U_j(t)$ are the errors of measurement.

3.3. L_∞ Performance and the Stability of the Control Scheme

Let the errors from the output and input of the first-order low-pass filters be expressed as

$$\begin{aligned} y_{i,2} &= z_{i,2} - \bar{v}_{i,(0,2)}, i = X, Y, Z, \\ y_{2*j} &= z_{2*j} - x_{(2*j)d}, j = 1, 2, 3. \end{aligned} \tag{49}$$

One has

$$\dot{y}_{i,2} = -\frac{y_{i,2}}{\tau_{i,2}} + \left(l_{i,1} \dot{S}_{i,1} + k_i \dot{\varsigma}_{i,(0,2)} + \left[k_i \dot{\hat{\vartheta}}_i \Xi_{i,(2)}^T \right]' - \ddot{y}_{ri} \right) / k_i \tag{50}$$

$$\dot{y}_{2*j} = -\frac{y_{2*j}}{\tau_{2*j}} + k_{2*j-1} \dot{S}_{2*j-1} - \ddot{x}_{(2*j-1)r}. \tag{51}$$

Then, we have

$$\left|\dot{y}_{i,2} + \frac{y_{i,2}}{\tau_{i,2}}\right| \leq B_{i,2}\left(S_{i,1}, y_{i,2}, \tilde{\vartheta}_i, y_{ri}, \dot{y}_{ri}, \ddot{y}_{ri}\right), \tag{52}$$

$$\left|\dot{y}_{2*j} + \frac{y_{2*j}}{\tau_{2*j}}\right| \leq B_{2*j}\left(S_{2*j-1}, y_{2*j}, \ddot{x}_{(2*j-1)r}\right), \tag{53}$$

where $B_{i,2}$ and B_{2*j} are continuous functions.

Then, from (25) and (26), (30), (36), (40) and (42), one has

$$S_{i,1}\dot{S}_{i,1} = -l_{i,1}S_{i,1}^2 + k_i S_{i,1}(S_{i,2}+y_{i,2}) - \tilde{\vartheta}_i^T \Xi_{i,(2)}^T S_{i,1} + \epsilon_{i,2}S_{i,1} \tag{54}$$

$$S_{i,2}\dot{S}_{i,2} = -k_i q_{i,2} v_{i,(0,1)} S_{i,2} - \dot{z}_2 S_{i,2} + k_i^{-1} U_i S_{i,2} \tag{55}$$

$$S_{2*j-1}\dot{S}_{2*j-1} = S_{2*j-1}(S_{2*j} - k_{2*j-1}S_{2*j-1}) + S_{2*j-1}y_{2*j} \tag{56}$$

$$S_{2*j}\dot{S}_{2*j} = S_{2*j}\left(\Theta_{\alpha_j}^T \Gamma_{\alpha_j} + U_j + d_j(t) - \dot{z}_{2*j}\right) \tag{57}$$

wherein $i = X, Y, Z, j = 1, 2, 3$, $\epsilon_{i,2}$, denoting the second row of ϵ_i. Then, we can obtain the Lyapunov function as:

$$V = \sum\left(\tfrac{1}{2}S_{i,1}^2 + \tfrac{1}{2}S_{i,2}^2 + \tfrac{1}{2}y_{i,2}^2 + \tfrac{1}{2r_{\vartheta_i}}\tilde{\vartheta}_i^T\tilde{\vartheta}_i + V_{\epsilon_i}\right) + \sum_{j=1}^{6}\tfrac{1}{2}S_j^2 + \sum_{j=1}^{3}\left(\tfrac{1}{2r_{\Theta_{\alpha_j}}}\tilde{\Theta}_{\alpha_j}^2 + \tfrac{1}{2}y_{2*j}^2\right). \tag{58}$$

Therein, $\tilde{\Theta}_{\alpha_j} = \hat{\Theta}_{\alpha_j} - \Theta_{\alpha_j}$, $\tilde{\vartheta}_i = \hat{\vartheta}_i - \vartheta_i^*$, $i = X, Y, Z$, and $j = 1, 2, 3$ denote the estimation errors.

Combining the results of the above control schemes, we can observe the following.

Theorem 1: According to the quadrotor model given in (10) and the adaptive control laws containing the unknown parameters in (27) and (46), as well as the actual control signals obtained through the event-triggered mechanism in (32) and (47), if $V(0)$ in (58) satisfies $V(0) \leq G_1$, wherein G_1 can be arbitrarily given as a positive number, then all signals in the quadrotor systems are semi-globally uniformly and ultimately bounded, which can be made arbitrarily small by choosing the fitness design parameters k_i, $l_{i,1}$, $l_{i,2}$, r_{ϑ_i}, σ_{ϑ_i}, k_{2*j-1}, k_{2*j}, $r_{\Theta_{\alpha_j}}$, $\sigma_{\Theta_{\alpha_j}}$, along with the time constants $\tau_{i,2}$, as well as τ_{2*j} In addition, the L_∞ norm of the tracking errors $S_{i,1}$, S_{2*j-1}, $i = X, Y, Z$, $j = 1, 2, 3$ can be made arbitrarily small by applying the technique of initialization.

Theorem 1. *In the event triggering mechanism, there must be a time interval $t' > 0$ satisfying $t_{n+1} - t_n > t'$, $\forall n \in \mathbb{Z}^+$, which indicates that the time interval has a lower bound.*

Proof. Please see the details about Theorem 2 in Appendix A. □

4. Experiments

The hardware-loop platform was used for testing the proposed control method. Figures 3 and 4 show the environment used for the actual experiment and the structure of the experimental system, respectively, where the following components were included: (1) a rapid control prototype (RCP), (2) a real-time simulator (RTS), (3) an adapter plate, and (4) a host computer.

Remark 2. *It should be noted that the control system was implemented in the hardware-in-loop simulation stage, as shown in Figure 3 (page 12), where the whole experimental platform was composed of four parts, namely, a real-time simulator (RTS), a rapid control prototype (RCP), an adapter plate, and a host computer. Compared with simulations conducted only on a host computer, hardware in the loop simulations are closer to actual physical control experiments conducted in real-world applications. In future works we will focus on field-testing the control of quadrotor UARs in the real world.*

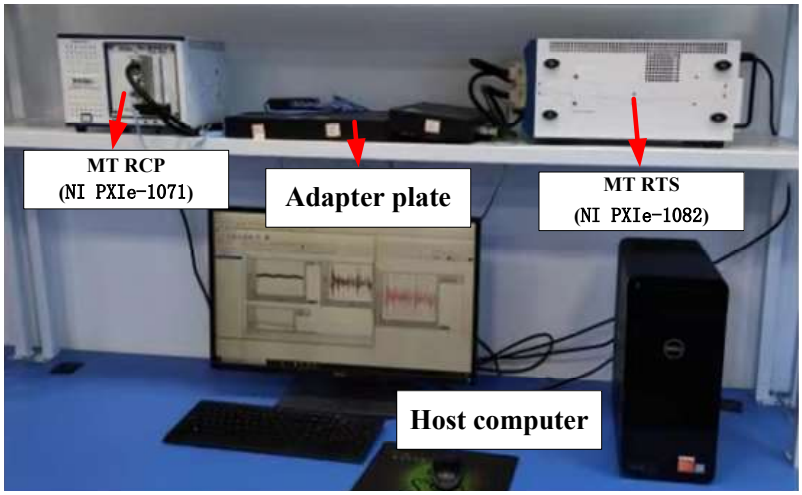

Figure 3. The environment used for the actual experiment.

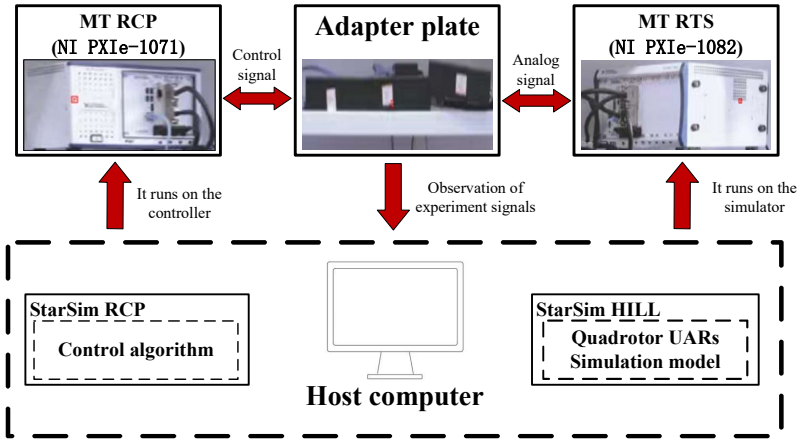

Figure 4. The structure of the experimental system.

In the experiment, the reference trajectories $\{X_d, Y_d, Z_d, \psi_d\}$ were selected as $\{\cos(t), \sin(t), 0.5t, 0\}$. The parameters of the control model are shown in Table 2.

Table 2. The design parameters of the quadrotor.

Symbol	Value	Units
m	1.4	kg
k	2.98	$10^{-6}\mathrm{N}\cdot\mathrm{s}^2\cdot\mathrm{rad}^{-2}$
l	0.2	m
τ	1.14	$10^{-7}\mathrm{N}\cdot\mathrm{s}^2\cdot\mathrm{rad}^{-2}$
d_ϕ, d_θ, d_ψ	1.2	$10^{-2}\mathrm{N}\cdot\mathrm{s}^2\cdot\mathrm{rad}^{-2}$
J_x	1.8	$\mathrm{N}\cdot\mathrm{s}^2\cdot\mathrm{rad}^{-2}$
J_y	1.8	$\mathrm{N}\cdot\mathrm{s}^2\cdot\mathrm{rad}^{-2}$
J_z	2.4	$\mathrm{N}\cdot\mathrm{s}^2\cdot\mathrm{rad}^{-2}$

Remark 3. *It should be noted that the instantaneous position of the quadrotor can be tracked accurately by looking for the experimental data at the corresponding time, and the real-time control based on the DSC method can also be achieved on the hardware-in-loop simulation platform.*

For the high-gain-state observer in (13) we have $A_{i,0} = \begin{bmatrix} -q_{i,1} & 1 \\ -q_{i,2} & 0 \end{bmatrix}$, $q_1 = q_2 = \begin{bmatrix} 5 \\ 3 \end{bmatrix}$, $q_3 = \begin{bmatrix} 1 \\ 10 \end{bmatrix}$, $k_i = 2$, $\Delta_i^{-1} = \begin{bmatrix} 1 & 0 \\ 0 & 1/k_i \end{bmatrix}$, $i = X, Y, Z$.

The control algorithm parameters were chosen as follows: $l_{X,1} = 16$, $l_{Y,1} = 56$, $l_{Z,1} = 10$, $l_{X,2} = 48$, $l_{Y,2} = 168$, $l_{Z,2} = 100$, $k_1 = 20$, $k_2 = 60$, $k_3 = 20$, $k_4 = 60$, $k_5 = 10$, $k_6 = 26$, $\gamma_{\vartheta_X} = \gamma_{\vartheta_Y} = \gamma_{\vartheta_Z} = 3$, $\sigma_{\vartheta_X} = \sigma_{\vartheta_Y} = \sigma_{\vartheta_Z} = 0.5$, $r_{\Theta_{\alpha_1}} = 2$, $r_{\Theta_{\alpha_2}} = 0.02$, $r_{\Theta_{\alpha_3}} = 0.5$, $\sigma_{\Theta_{\alpha_1}} = 0.1$, $\sigma_{\Theta_{\alpha_2}} = 0.002$, $\sigma_{\Theta_{\alpha_3}} = 0.2$, $g_{X,1} = 1$, $\rho_X = 0.02$, $g_X = 0.001$, $g_{Y,1} = 3$, $\rho_Y = 0.05$, $g_Y = 0.001$, $g_{Z,1} = 2$, $\rho_Z = 0.06$, $g_Z = 0.001$, $\delta_1 = \delta_2 = 0.005$, $\bar{\psi}_1 = \bar{\psi}_2 = 6$, $\psi_1 = \psi_2 = 0.05$, $\beta_1 = \beta_2 = 8$, $\delta_3 = 0.02$, $\bar{\psi}_3 = 0.0002$, $\psi_3 =, 0.08$, $\beta_3 = 0.0001$. In addition, we included the time constants of a low-pass filter: $\tau_{X,2} = \tau_{Y,2} = \tau_{Z,2} = \tau_2 = \tau_4 = \tau_6 = 0.05$.

For the design of the position controller, the RBFNNs $\psi_i(\xi_i), i = X, Y, Z$ all had seven nodes. The centers of the base functions were –1, –0.8, –0.4, 0, 0.4, 0.8, 1, with the corresponding width $\eta_{i,n}, n = 1 \ldots 7$ and with $\xi_i = \left(\hat{\dot{x}}_{i,2}\right)$. Furthermore,

$$\begin{aligned} \Psi_i^T(\xi) &= \begin{bmatrix} 0 & 0 \\ 0 & \psi_{i,2}(\xi_i) \end{bmatrix} \\ &= \begin{bmatrix} 0 & 0 \\ 0 & \psi_{i1,1}(\xi_{i,1}), \ldots, \psi_{i1,7}(\xi_{i,1}) \end{bmatrix} \end{aligned} \tag{59}$$

According to [12], a comparative simulation which combined the BSMC scheme and the event-triggering mechanism was conducted.Moreover, the same model parameters and external disturbance of the quadrotor were also applied. Then, the tracking effects and tracking errors of the reference trajectories for the two methods, as well as the parameters of the control signal and the adaptive law, were presented in the simulation. Then, the reference trajectories of the roll and pitch angle were designed in the process of the control scheme. Thus, different control schemes would result in different attitude angle reference trajectories.

The experimental results of the positioning trajectory tracking are presented in Figures 5–8 and the attitude tracking and errors are presented in Figures 9–11. The control performance of the model presented in this paper can be observed in Figures 6–11. Smaller tracking errors and a better tracking performance could be obtained compared to the BSMC method. Figure 12 presents the actual control signals U_1 to U_4, and Figure 13 shows the control signals U_X, U_Y, U_Z obtained in position tracking. As can be seen in Figures 12 and 13, the updated frequencies of control signals were significantly reduced after the introduction of the event triggering mechanism. Figure 14 depicts the estimated values of $\vartheta_X, \vartheta_Y, \vartheta_Z$ and the unknown parameters $\hat{\vartheta}_X, \hat{\vartheta}_Y, \hat{\vartheta}_Z$. In addition to evaluating the accuracy of the proposed scheme, the mean average error $MAE = \sum_{i=i_{ss}}^{N} |S_1(i)|/(N - i_{ss}), N = 20,000, i_{ss} = 12{,}000$ and the root mean squared error $RMSE = \sqrt{\sum_{i=i_{ss}}^{N} S_1^2(i)/(N - i_{ss})}, N = 20,000, i_{ss} = 12{,}000$ were selected as metrics for study. The MAE and RMSE of the designed control strategy, as well as those of BSMC, are presented in Tables 3 and 4.

Table 3. MAE and RMSE of position tracking.

Scheme	MAE			RMSE		
	X	**Y**	**Z**	**X**	**Y**	**Z**
BSMC	0.427%	1.247%	0.779%	0.520%	1.344%	0.845%
Our proposed method	0.092%	0.156%	0.322%	0.104%	0.171%	0.352%

Table 4. MAE and RMSE of angle tracking.

Scheme	MAE			RMSE		
	$\boldsymbol{\phi}$	$\boldsymbol{\theta}$	$\boldsymbol{\psi}$	$\boldsymbol{\phi}$	$\boldsymbol{\theta}$	$\boldsymbol{\psi}$
BSMC	2.258%	2.288%	1.137×10^{-6}	2.264%	2.299 %	1.306×10^{-6}
Our proposed method	0.082%	0.098%	1.148×10^{-8}	0.093%	0.108%	1.282×10^{-8}

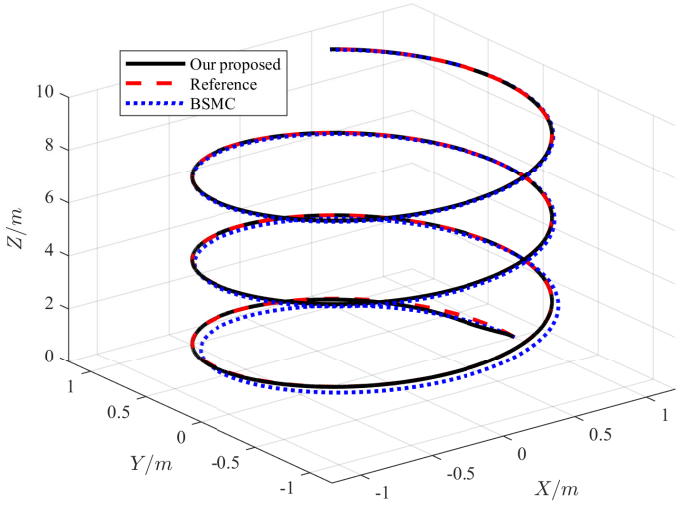

Figure 5. Diagram of the control performance in space.

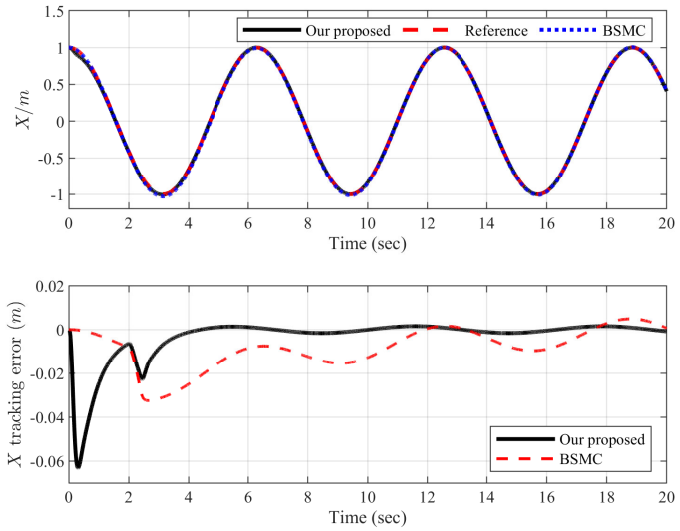

Figure 6. The control performance and tracking errors in relation to x.

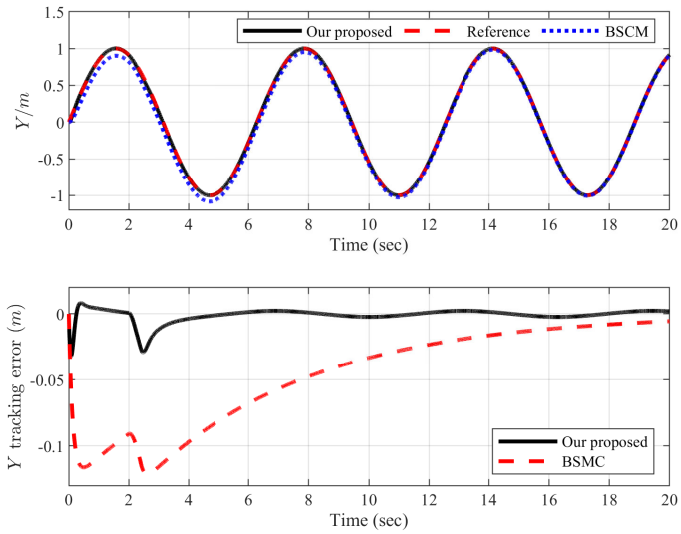

Figure 7. The control performance and tracking errors in relation to y.

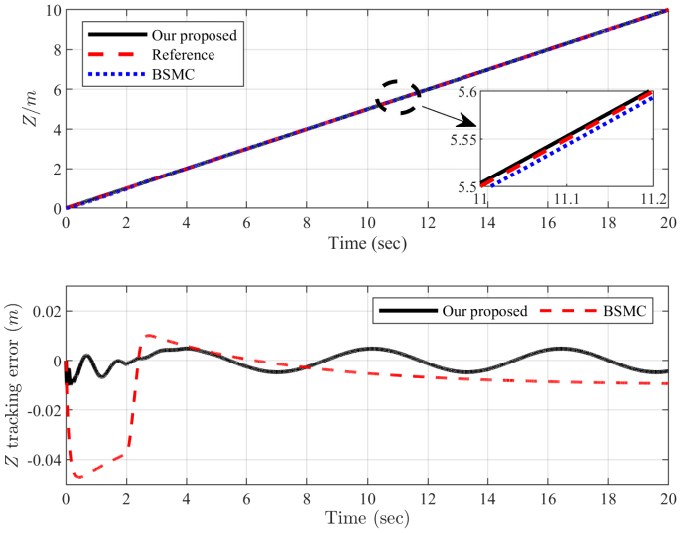

Figure 8. The control performance and tracking errors in relation to z.

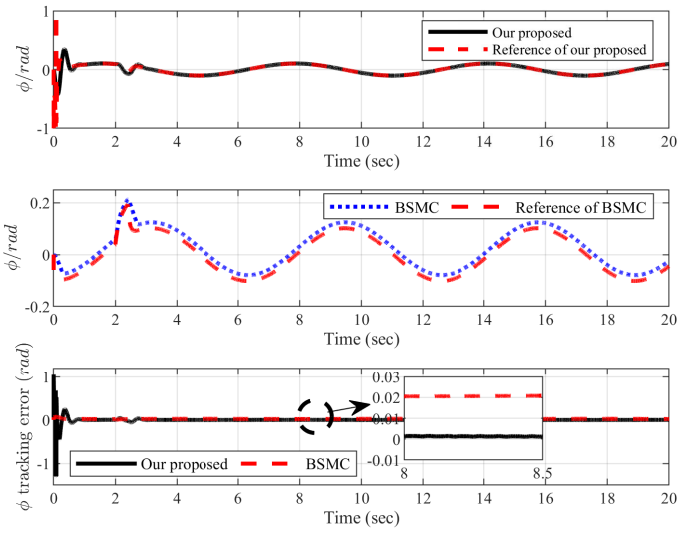

Figure 9. The control performance and tracking errors in relation to the roll angle.

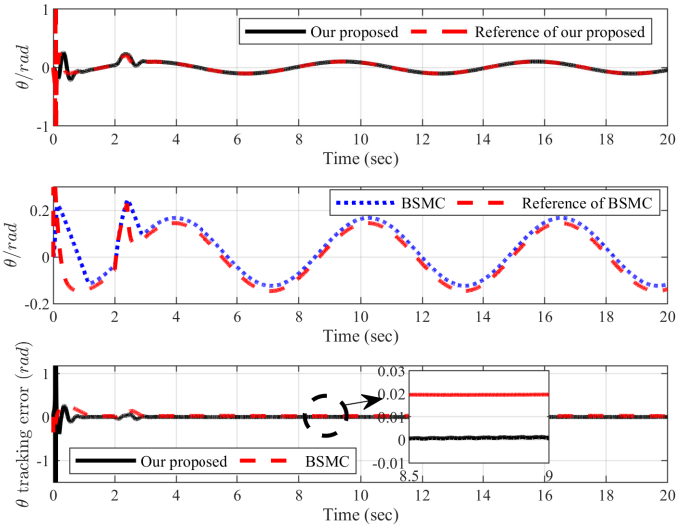

Figure 10. The tracking performance and tracking errors in relation to the pitch angle.

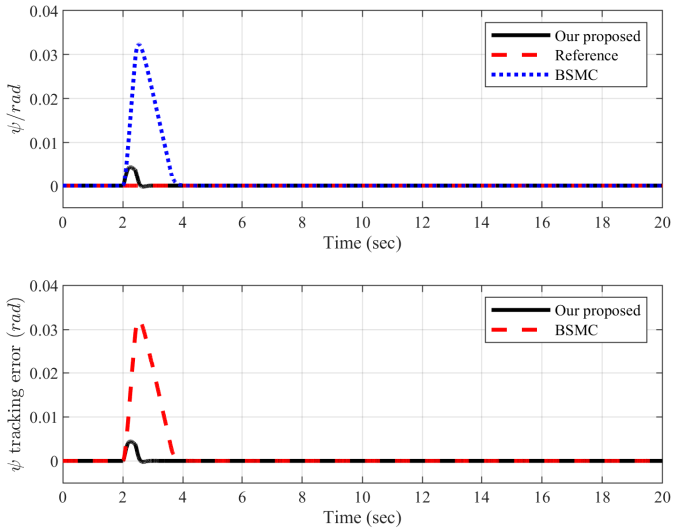

Figure 11. The control performance and tracking errors in relation to the yaw angle.

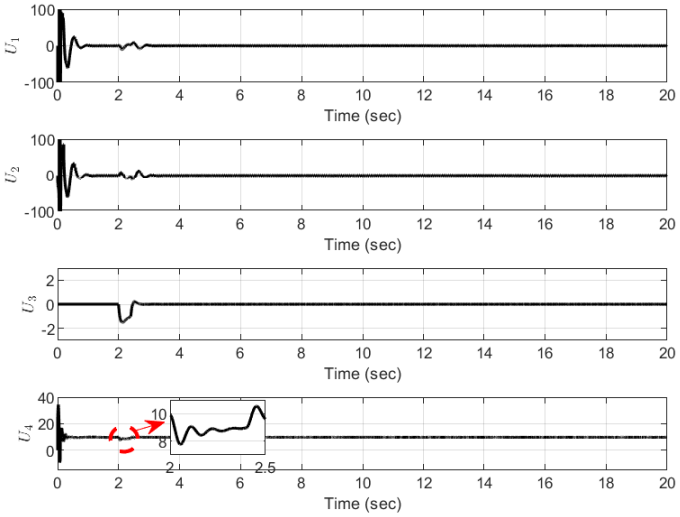

Figure 12. Control signals U_1 to U_4.

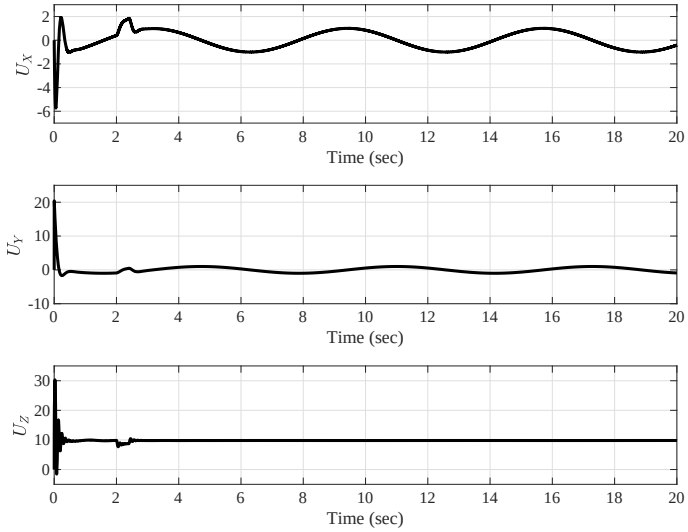

Figure 13. The control signals.

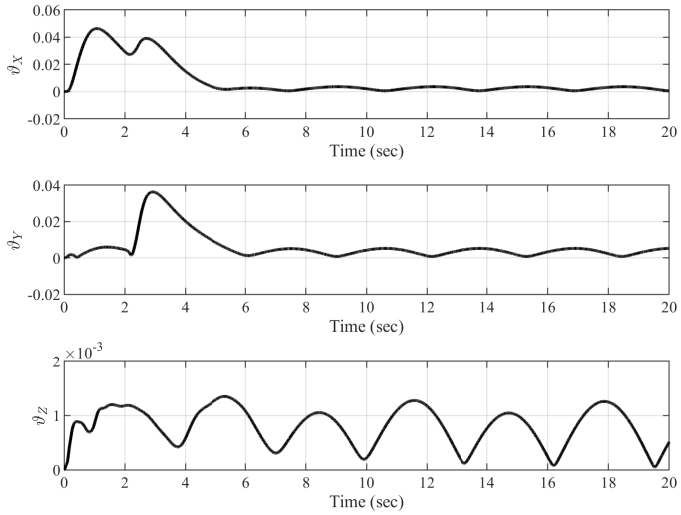

Figure 14. The estimation of adaptive parameters $\vartheta_X, \vartheta_Y, \vartheta_Z$.

5. Conclusions

A neural network and event-triggered-mechanism-based adaptive control method for the tracking control of a quadrotor UAR's trajectory was proposed in this study. The system stability analysis and the experimental results showed that: (1) The unmeasurable state in the system was estimated by constructing a high gain filter observer, combined with the output feedback method. Under conditions in which position information was available, the "differential explosion" problem was overcome by means of a DSC control scheme, and good performance was obtained. (2) The update signal of the frequency was reduced by using the event-triggering control method properly and the robustness of our proposed method was tested. (3) The L_∞ tracking performance of the system was achieved by adopting the initialization technique and choosing the appropriate controller parameters. (4) Based on the outcomes of the hardware-in-loop simulation, we observed that our proposed control method exhibited good performance compared to that of the BSMC scheme. The proposed scheme provided 0.335%, 1.091%, 0.457%, 2.176%, 2.19%, and 1.126×10^{-6} lower mean average error (MAE) values compared to those of the BSMC algorithm in relation to X, Y, Z, ϕ, θ, and ψ, respectively.

Author Contributions: Conceptualization, X.Z. and G.Z.; methodology, C.-Y.S.; software, M.L.; validation, P.L. and M.L.; formal analysis, P.L. and M.L.; investigation, P.L. and M.L.; data curation, P.L. and M.L.; writing—original draft preparation, P.L. and M.L.; writing—review and editing, X.Z.; visualization, P.L. and M.L.; supervision, X.Z., G.Z. and Z.L.; project administration, X.Z. and G.Z.; funding acquisition, X.Z. and G.Z. All authors have read and agreed to the published version of the manuscript.

Funding: This research was funded by the Science and Technology Research Project of Education Department of Jilin Province grant number JJKH20220115KJ; Science and Technology Project of Jilin Province grant number 20210509053RQ; Innovation and Entrepreneurship Talent Funding Project of Jilin Province grant number 2021Y005.

Institutional Review Board Statement: Not applicable.

Informed Consent Statement: Not applicable.

Data Availability Statement: Not applicable.

Conflicts of Interest: The authors declare no conflict of interest.

Appendix A

Appendix A.1. Proof of Lemma 2

Define the following error transfer function:

$$\hat{\epsilon}_i = \Delta_i^{-1}\epsilon_i \tag{A1}$$

$$\dot{\hat{\epsilon}}_i = k_i A_{i,0}\hat{\epsilon}_i + \Delta_i^{-1}B_i \tag{A2}$$

$$\hat{\hat{x}}_i = \Delta_i \varsigma_{i,0} + \Delta_i v_{i,0} + \Delta_i \Xi_i \hat{\vartheta}_i. \tag{A3}$$

where $A_{i,0}$ denotes a Hurwitz matrix, and $\bar{P}_i$ is the symmetric positive definite matrix that makes Equation (20) true and defines the quadratic function

$$V_{\hat{\epsilon}_i} = \hat{\epsilon}_i^T \bar{P}_i \hat{\epsilon}_i. \tag{A4}$$

$$\begin{aligned} \dot{V}_{\hat{\epsilon}_i} &= -2k_i \hat{\epsilon}_i^T \hat{\epsilon}_i + 2\hat{\epsilon}_i^T \bar{P}_i \Delta_i^{-1} B_i \\ &\leq -2k_i \|\hat{\epsilon}_i\|^2 + 2\|\hat{\epsilon}_i\| \|\bar{P}_i\| \|B_i\|_{\max}/k_i. \end{aligned} \tag{A5}$$

Through Young's inequality, we can further obtain

$$\begin{aligned} \dot{V}_{\hat{\epsilon}_i} &\leq -2k_i \|\hat{\epsilon}_i\|^2 + k_i \|\hat{\epsilon}_i\|^2 + 2k_i \left(\frac{\|\bar{P}_i\| \|B_i\|_{\max}}{k_i^2}\right)^2 \\ &\leq -\frac{k_i}{\lambda_{\max}(\bar{P}_i)} \hat{\epsilon}_i^T \bar{P}_i \hat{\epsilon}_i + 2k_i \left(\frac{\|\bar{P}_i\| \|B_i\|_{\max}}{k_i^2}\right)^2 \end{aligned} \tag{A6}$$

where $\lambda_{\max}(\bar{P}_i)$ denotes the maximum eigenvalue of $\bar{P}_i$.

It follows that

$$V_{\epsilon_i} = \epsilon_i^T P_i \epsilon_i = \hat{\epsilon}_i^T \bar{P}_i \hat{\epsilon}_i = V_{\hat{\epsilon}_i}, \forall t \geq 0. \tag{A7}$$

Appendix A.2. Proof of Theorem 1

Define

$$\begin{aligned} \Omega_{i,1} &= \left\{ (y_{ri}, \dot{y}_{ri}, \ddot{y}_{ri}) : y_{ri}^2 + \dot{y}_{ri}^2 + \ddot{y}_{ri}^2 \leq G_{i,0} \right\} \\ \Omega_{i,2} &= S_{i,1}^2 + S_{i,2}^2 + y_{i,2}^2 + \frac{1}{r_{\vartheta_i}} \tilde{\vartheta}_i^2 + 2\epsilon_i^T P_i \epsilon_i \leq 2p \\ \Pi_{j,1} &= \left\{ (y_{rj}, \dot{y}_{rj}, \ddot{y}_{rj}) : y_{rj}^2 + \dot{y}_{rj}^2 + \ddot{y}_{rj}^2 \leq H_{i,0} \right\} \\ \Pi_{j,2} &= S_{2*j-1}^2 + S_{2*j}^2 + y_{2*j}^2 + \frac{1}{r_{\Theta_{\alpha_j}}} \tilde{\Theta}_{\alpha_j}^2 \leq 2p' \end{aligned} \tag{A8}$$

with $G_{i,0}$ and $H_{i,0}$ being positive constants. In the compact $\Omega_{i,1} \times \Omega_{i,2}$, the continuous function $B_{i,2}$ has the maximum value $M_{i,2}, i = X, Y, Z$. Then, $\dot{V}$ in (58); it follows that

$$\begin{aligned} \dot{V} = &\sum \left(S_{i,1}\dot{S}_{i,1} + S_{i,2}\dot{S}_{i,2} + y_{i,2}\dot{y}_{i,2} + \frac{1}{r_{\vartheta_i}} \tilde{\vartheta}_i^T \dot{\tilde{\vartheta}}_i + \dot{V}_{\epsilon_i} \right) \\ &+ \sum_{j=1}^{6} S_j \dot{S}_j + \sum_{j=1}^{3} \left(\frac{1}{r_{\Theta_{\alpha_j}}} \tilde{\Theta}_{\alpha_j}^T \dot{\tilde{\Theta}}_{\alpha_j} + y_{2*j}\dot{y}_{2*j} \right). \end{aligned} \tag{A9}$$

By using (52) and (53), we arrive at

$$\begin{aligned} y_{i,2}\dot{y}_{i,2} &\leq -\frac{y_{i,2}^2}{\tau_{i,2}} + \frac{y_{i,2}^2 M_{i,2}^2}{2\kappa_i} + \frac{\kappa_i}{2} \\ y_{2*j}\dot{y}_{2*j} &\leq -\frac{y_{2*j}^2}{\tau_{2*j}} + \frac{y_{2*j}^2 M_{2*j}^2}{2\upsilon_{2*j}} + \frac{\upsilon_{2*j}}{2} \end{aligned} \tag{A10}$$

where κ_i and υ_{2*j} are positive constants.

Since $\hat{\epsilon}_i = \Delta_i^{-1}\epsilon_i$, we have $\epsilon_{i,2}^2 = k_i^2\hat{\epsilon}_{i,2}^2 \leq \left[k_i^2/\lambda_{\min}(\bar{P}_i)\right]V_{\hat{\epsilon}_i} = \left[k_i^2/\lambda_{\min}(\bar{P}_i)\right]V_{\epsilon_i}$. Using Young's inequality, we can see that

$$S_{i,1}\epsilon_{i,2} \leq \frac{k_i^2}{2}S_{i,1}^2 + \frac{1}{\lambda_{\min}(\bar{P}_i)}V_{\epsilon_i}. \tag{A11}$$

From (25), (56) and (A11), we can conclude that

$$S_{i,1}\dot{S}_{i,1} \leq -\left(l_{i,1} - \frac{k_i}{2} - \frac{k_i^2}{2}\right)S_{i,1}^2 + \frac{k_i}{2}y_{i,2}^2 + k_i S_{i,1}S_{i,2} - \tilde{\vartheta}_i^T k_i \Xi_{i,(2)}^T S_{i,1} + \frac{1}{2\lambda_{\min}(\bar{P}_i)}V_{\epsilon_i} \tag{A12}$$

$$S_{2*j-1}\dot{S}_{2*j-1} \leq -(k_{2*j-1} - 1)S_{2*j-1}^2 + \frac{1}{2}S_{2*j}^2 + \frac{1}{2}y_{2*j}^2. \tag{A13}$$

Similarly, using (30), one observes that

$$S_{i,2}\dot{S}_{i,2} = -k_i q_{i,2} v_{i,(0,1)} S_{i,2} + k_i^{-1}U_i S_{i,2} - \dot{z}_2 S_{i,2} \tag{A14}$$

For $\forall t \in [t_j, t_{j+1})$, we have

$$\left|\breve{U}_i(t) - U_i(t)\right| \leq g, \tag{A15}$$

and there is always a $\lambda(t)$ satisfying $\lambda(t_j) = 0, \lambda(t_{j+1}) = \pm 1$, that is, $|\lambda(t)| \leq 1$, and thus, (A15) with:

$$\breve{U}_i(t) = U_i(t) + \lambda(t)g. \tag{A16}$$

From (A14) and (A16), one can observe that

$$S_{i,2}\dot{S}_{i,2} = -k_i q_{i,2} v_{i,(0,1)} S_{i,2} + k_i^{-1}S_{i,2}\left(\breve{U}_i(t) - \lambda(t)g\right) - \dot{z}_2 S_{i,2} \tag{A17}$$

Substituting (32) into (A17), it follows that:

$$S_{i,2}\dot{S}_{i,2} = -l_{i,2}S_{i,2}^2 + k_i^{-1}S_{i,2}\left(-g_1 \tanh\left(\frac{k^{-1}S_{i,2}g_1}{\rho}\right) - \lambda(t)g\right). \tag{A18}$$

Note that $tanh(\cdot)$ denotes the hyperbolic tangent function, which has the following characteristics:

$$0 \leq |\alpha| - \alpha \tanh\left(\frac{\alpha}{\beta}\right) \leq 0.2785\beta \tag{A19}$$

where $\alpha > 0, \beta \in R$. From (A18) and (A19), it follows that

$$S_{i,2}\dot{S}_{i,2} \leq -l_{i,2}S_{i,2}^2 + 0.2785\beta. \tag{A20}$$

In the same way, we have:

$$S_{2*j}\dot{S}_{2*j} \leq -k_{2*j}S_{2*j}^2 - \frac{1}{2}S_{2*j}^2 - \tilde{\Theta}_{\alpha_j}^T \Gamma_{\alpha_j} S_{2*j} + \frac{1}{2}d_j^2(t) + 0.2785\rho. \tag{A21}$$

Noting the adaptive law (27), it follows that:

$$\begin{aligned}\frac{1}{r_{\vartheta_i}}\tilde{\vartheta}_i^T\dot{\hat{\vartheta}}_i &= \tilde{\vartheta}_i^T k_i \Xi_{i,(2)}^T S_{i,1} - \sigma_{\vartheta_i}\tilde{\vartheta}_i^T\hat{\vartheta}_i \\ \frac{1}{r_{\Theta_{\alpha_j}}}\tilde{\Theta}_{\alpha_j}^T\dot{\hat{\Theta}}_{\alpha_j} &= \tilde{\Theta}_{\alpha_j}^T\Gamma_{\alpha_j}S_{2*j} - \sigma_{\Theta_{\alpha_j}}\tilde{\Theta}_{\alpha_j}^T\hat{\Theta}_{\alpha_j}\end{aligned} \tag{A22}$$

According to the definition of $\tilde{\vartheta}_i$ and $\hat{\Theta}_{\alpha_j}$, we can observe that

$$\begin{aligned}-\sigma_{\vartheta_i}\tilde{\vartheta}_i^T\hat{\vartheta}_i &= -\sigma_{\vartheta_i}\tilde{\vartheta}_i^T\left(\tilde{\vartheta}_i+\vartheta_i^*\right) \le -\frac{\sigma_{\vartheta_i}}{2}\tilde{\vartheta}_i^T\tilde{\vartheta}_i + \frac{\sigma_{\vartheta_i}}{2}\vartheta_i^{*T}\vartheta_i^* \\ -\sigma_{\Theta_{\alpha_j}}\tilde{\Theta}_{\alpha_j}^T\hat{\Theta}_{\alpha_j} &= -\sigma_{\Theta_{\alpha_j}}\tilde{\Theta}_{\alpha_j}^T\left(\tilde{\Theta}_{\alpha_j}+\Theta_{\alpha_j}\right) \le -\frac{\sigma_{\Theta_{\alpha_j}}}{2}\tilde{\Theta}_{\alpha_j}^T\tilde{\Theta}_{\alpha_j} + \frac{\sigma_{\Theta_{\alpha_j}}}{2}\Theta_{\alpha_j}^T\Theta_{\alpha_j}.\end{aligned} \tag{A23}$$

Substituting (A10), (A13), (A20), and (A21)–(A23) into (A9), it follows that:

$$\begin{aligned}\dot{V} \le \sum\Bigg[&-\left(l_{i,1}-k_i-\tfrac{k_i^2}{2}\right)S_{i,1}^2-\left(l_{i,2}-\tfrac{k_i}{2}\right)S_{i,2}^2-\tfrac{\sigma_{\vartheta_i}}{2}\tilde{\vartheta}_i^T\tilde{\vartheta}_i+\tfrac{\sigma_{\vartheta_i}}{2}\vartheta_i^{*T}\vartheta_i^* \\ &+\left(\tfrac{k_i}{2}-\tfrac{1}{\tau_{i,2}}+\tfrac{M_{i,2}^2}{2\kappa_i}\right)y_{i,2}^2+0.8355\beta+\left(\tfrac{1}{2\lambda_{\min}(\bar{P}_i)}-\tfrac{k_i}{\lambda_{\max}(\bar{P}_i)}\right)V_{\epsilon_i} \\ &+2k_i\left(\tfrac{\|\bar{P}_i\|\|B_i\|_{\max}}{k_i^2}\right)^2\Bigg]+\sum_{j=1}^{3}\Bigg[-(k_{2*j-1}-1)S_{2*j-1}^2-k_{2*j}S_{2*j}^2+\tfrac{1}{2}y_{2*j}^2 \\ &+\tfrac{1}{2}d_j^2(t)-\tfrac{\sigma_{\Theta_{\alpha_j}}}{2}\tilde{\Theta}_{\alpha_j}^T\tilde{\Theta}_{\alpha_j}+\tfrac{\sigma_{\Theta_{\alpha_j}}}{2}\Theta_{\alpha_j}^T\Theta_{\alpha_j}-\tfrac{y_{2*j}^2}{\tau_{2*j}}+\tfrac{y_{2*j}^2M_{2*j}^2}{2v_{2*j}}+\tfrac{v_{2*j}}{2}+0.8355\rho\Bigg].\end{aligned} \tag{A24}$$

By choosing the following design parameters:

$$\begin{aligned}k_i &\ge 2\lambda_{\max}(\bar{P}_i)c_{i,1}+\lambda_{\max}(\bar{P}_i)/2\lambda_{\min}(\bar{P}_i) \\ l_{i,1} &\ge k_i^2/2+k_i+c_{i,1} \\ l_{i,2} &\ge k_i/2+c_{i,1} \\ \frac{1}{\tau_{i,2}} &\ge k_i/2+M_{i,2}^2/(2\kappa_i)+c_{i,1} \\ \sigma_{\vartheta_i} &\ge 2c_{i,1}/r_{\vartheta_i} \\ c_{i,2} &= \sigma_{\vartheta_i}\vartheta_i^{*T}\vartheta_i^*/2+k_i/2+2k_i(\|\bar{P}_i\|\|B_i\|_{\max}/k_i^2)^2+0.8355\beta \\ 1/\tau_{2*j} &\ge 1/2+M_{2*j}^2/(2v_{2*j})+c_{j,1} \\ k_{2*j-1} &\ge 1+c_{j,1} \\ k_{2*j} &\ge c_{j,1} \\ \sigma_{\Theta_{\alpha_j}} &\ge 2c_{j,1}/r_{\Theta_{\alpha_j}} \\ c_{j,2} &= \sigma_{\Theta_{\alpha_j}}\Theta_{\alpha_j}^T\Theta_{\alpha_j}/2+v_{2*j}/2+d_j^2(t)/2+0.8355\rho\end{aligned} \tag{A25}$$

where $c_{i,1}$ and $c_{j,1}$ satisfy $c_{i,1} \ge c_{i,2}/(2G_1)$ and $c_{j,1} \ge c_{j,2}/(2G_1)$, $i = X, Y, Z$, $j = 1, 2, 3$, respectively. According to (A24), one has

$$\dot{V} \le -2C_1V + C_2 \tag{A26}$$

where $C_1 = \min\{c_{X,1}, c_{Y,1}, c_{Z,1}, c_{1,1}, c_{2,1}, c_{3,1}\}$, $C_2 = c_{X,2}+c_{Y,2}+c_{Z,2}+c_{1,2}+c_{2,2}+c_{3,2}$. It can be seen that $\dot{V} \le 0$, whereas $V = G_1$, which means that $V(t) \le G_1$ is an invariant set. For all $t \ge 0$, if $V(0) \le G_1$, there must be $V(t) \le G_1$. Therefore, V is uniformly bounded. By solving the inequality in (A26), we have:

$$V(t) \le C_2/(2C_1)+e^{-2C_1t}[V(0)-C_2/(2C_1)], \forall t \ge 0, \tag{A27}$$

which implies that $\lim_{t\to\infty} V(t) \le C_2/(2C_1)$. It should be noted that the value of C_1 in (A26) is chosen based on the minimum value of $c_{i,1}, i = X, Y, Z, 1, 2, 3$. This indicates that when the above design parameters values are large enough, a large enough value of C_1 can be obtained.Thus, C_2 is a constant defined in (A26), meaning that $C_2/(2C_1)$ can also be small enough.

In order to obtain L_∞ tracking performance, let:

$$\begin{aligned} y_{ri}(0) &= y_i(0) \\ S_{i,1}(0) &= 0 \\ v_{i,0}(0) &= 0 \\ \varsigma_{i,(0,1)}(0) &= 0 \\ \Xi_i(0) &= 0 \\ \hat{\vartheta}_i(0) &= 0 \\ S_{2*j-1}(0) &= 0 \\ \hat{\Theta}_{\alpha_j}(0) &= 0 \\ x_{(2*j-1)r}(0) &= x_{2*j-1}(0). \end{aligned} \tag{A28}$$

where $\varsigma_{i,(0,1)}(0) = y_i(0) = x_{i,1}(0)$. We have $V(t) \le C_2/(2C_1) + \sum \lambda_{\max}(\bar{P}_i)\|\epsilon_i(0)\|^2/k_i^2$, $i = X, Y, Z$. According to (A24), we have $\left\|S_{2*j-1}\right\|_\infty = \sup_{t\ge 0}\left|S_{2*j-1}\right| = \|x_1 - x_{1r}\|_\infty \le \sqrt{C_2/(2C_1)}$, $\|S_{i,1}\|_\infty = \sup_{t\ge 0}|S_{i,1}| = \|x_{i,1} - y_{ri}\|_\infty \le \sqrt{C_2/(2C_1) + \sum \lambda_{\max}(\bar{P}_i)\|\epsilon_i(0)\|^2/k_i^2}$, $i = X, Y, Z, j = 1, 2, 3$, which means that the tracking error of L_∞ norm $\|S_{i,1}\|_\infty$, $\left\|S_{2*j-1}\right\|_\infty$, could be made arbitrarily small by selecting the appropriate parameters. The proof of Theorem 1 is completed.

Appendix A.3. Proof of Theorem 2

Take the event-triggered controller designed for the position subsystem as an example. Thus, we have $t \in [t_n, t_{n+1})$, from (33), wherein:

$$\frac{d}{dt}|e| = sign(e)\dot{e} \le \left|\dot{\breve{U}}_i(t)\right|. \tag{A29}$$

From (32), one has:

$$\dot{\breve{U}}_i(t) = \dot{U}_i(t) - \frac{g_{i,1}^2 k^{-1}}{\epsilon_i \cosh^2\left(\frac{k^{-1}S_{i,2}g_{i,1}}{\epsilon_i}\right)}. \tag{A30}$$

Since each item in (A30) is globally bounded, we can observe that $\dot{\breve{U}}_i(t)$ are continuous and bounded; that is, there must be $\mu > 0$ such that $\left|\dot{\breve{U}}_i(t)\right| \le \mu$. Furthermore, at t_n, $e(t_n) = 0$, as well as when $t \to t_{n+1}$, $e(t_{n+1}) = g_i$. Therefore, there must be a positive constant $t' = t_{n+1} - t_n$ that satisfies $t' > g_i/\mu$, which indicates that the time interval t' of event triggering has a lower bound; thus, Zeno behavior can be avoided. In the same way, the controller based on an event-triggered mechanism has been designed for attitude tracking, which can also effectively avoid the occurrence of Zeno behavior.

References

1. Shakhatreh, H.; Sawalmeh, A.H.; Al-Fuqaha, A.; Dou, Z.; Almaita, E.; Khalil, I.; Othman, N.S.; Khreishah, A.; Guizani, M. Unmanned aerial vehicles (UAVs): A survey on civil applications and key research challenges. *IEEE Access* **2019**, *7*, 48572–48634. [CrossRef]
2. Saeed, A.S.; Younes, A.B.; Cai, C.; Cai, G. A survey of hybrid unmanned aerial vehicles. *Prog. Aerosp. Sci.* **2018**, *98*, 91–105. [CrossRef]

3. Lu, Y.; Macias, D.; Dean, Z.S.; Kreger, N.R.; Wong, P.K. A UAV-mounted whole cell biosensor system for environmental monitoring applications. *IEEE Trans. Nanobiosci.* **2015**, *14*, 811–817. [CrossRef] [PubMed]
4. Zhang, X.; Lin, Y.; Wang, J. High-gain observer based decentralised output feedback control for interconnected nonlinear systems with unknown hysteresis input. *Int. J. Control.* **2013**, *86*, 1046–1059. [CrossRef]
5. Liu, H.; Zhao, W.; Zuo, Z.; Zhong, Y. Robust control for quadrotors with multiple time-varying uncertainties and delays. *IEEE Trans. Ind. Electron.* **2016**, *64*, 1303–1312. [CrossRef]
6. Wu, D.; Chen, X.; Yang, L.; Fu, G.; Shi, X. Compact and low-profile omnidirectional circularly polarized antenna with four coupling arcs for UAV applications. *IEEE Antennas Wirel. Propag. Lett.* **2017**, *16*, 2919–2922. [CrossRef]
7. Zhang, Y.; Chen, Z.; Zhang, X.; Sun, Q.; Sun, M. A novel control scheme for quadrotor UAV based upon active disturbance rejection control. *Aerosp. Sci. Technol.* **2018**, *79*, 601–609. [CrossRef]
8. Zhang, D.W.; Liu, G.P. Output feedback predictive control for discrete quasilinear systems with application to spacecraft flying-around. *Asian J. Control.* **2021**, *24*, 1846–1861. [CrossRef]
9. Yang, H.; Cheng, L.; Xia, Y.; Yuan, Y. Active disturbance rejection attitude control for a dual closed-loop quadrotor under gust wind. *IEEE Trans. Control. Syst. Technol.* **2017**, *26*, 1400–1405. [CrossRef]
10. Ma, Z.; Jiao, S.M. Research on the attitude control of quad-rotor UAV based on active disturbance rejection control. In Proceedings of the 2017 3rd IEEE International Conference on Control Science and Systems Engineering (ICCSSE), Beijing, China, 17–19 August 2017; pp. 45–49.
11. Li, S.; Wang, Y.; Tan, J.; Zheng, Y. Adaptive RBFNNs/integral sliding mode control for a quadrotor aircraft. *Neurocomputing* **2016**, *216*, 126–134. [CrossRef]
12. Chen, F.; Jiang, R.; Zhang, K.; Jiang, B.; Tao, G. Robust backstepping sliding-mode control and observer-based fault estimation for a quadrotor UAV. *IEEE Trans. Ind. Electron.* **2016**, *63*, 5044–5056. [CrossRef]
13. Xu, L.X.; Ma, H.J.; Guo, D.; Xie, A.H.; Song, D.L. Backstepping sliding-mode and cascade active disturbance rejection control for a quadrotor UAV. *IEEE/ASME Trans. Mechatron.* **2020**, *25*, 2743–2753. [CrossRef]
14. Almakhles, D.J. Robust backstepping sliding mode control for a quadrotor trajectory tracking application. *IEEE Access* **2019**, *8*, 5515–5525. [CrossRef]
15. Shi, X.; Hu, B.; Yin, C.; Cheng, Y.; Huang, X. Design of trajectory tracking controller with fractional-order backstepping sliding mode method for quadrotor UAV. In Proceedings of the 2018 Chinese Control And Decision Conference (CCDC), Shenyang, China, 9–11 June 2018; pp. 5960–5965.
16. Shao, X.; Liu, J.; Cao, H.; Shen, C.; Wang, H. Robust dynamic surface trajectory tracking control for a quadrotor UAV via extended state observer. *Int. J. Robust Nonlinear Control* **2018**, *28*, 2700–2719. [CrossRef]
17. Shen, Z.; Li, F.; Cao, X.; Guo, C. Prescribed performance dynamic surface control for trajectory tracking of quadrotor UAV with uncertainties and input constraints. *Int. J. Control* **2020**, *94*, 1–21. [CrossRef]
18. Muñoz, F.; González-Hernández, I.; Salazar, S.; Espinoza, E.S.; Lozano, R. Second order sliding mode controllers for altitude control of a quadrotor UAS: Real-time implementation in outdoor environments. *Neurocomputing* **2017**, *233*, 61–71. [CrossRef]
19. Nowzari, C.; Cortés, J. Distributed event-triggered coordination for average consensus on weight-balanced digraphs. *Automatica* **2016**, *68*, 237–244. [CrossRef]
20. Fan, Y.; Yang, Y.; Zhang, Y. Sampling-based event-triggered consensus for multi-agent systems. *Neurocomputing* **2016**, *191*, 141–147. [CrossRef]
21. You, X.; Hua, C.; Guan, X. Event-triggered leader-following consensus for nonlinear multiagent systems subject to actuator saturation using dynamic output feedback method. *IEEE Trans. Autom. Control.* **2018**, *63*, 4391–4396. [CrossRef]
22. Zeng, W.; Fan, H.; Wang, W. Event-triggered Adaptive Attitude Tracking Control of a Quadrotor UAV. In Proceedings of the 2019 Chinese Control And Decision Conference (CCDC), Nanchang, China, 3–5 June 2019; pp. 2855–2860.
23. Wang, C.; Guo, L.; Wen, C.; Hu, Q.; Qiao, J. Event-triggered adaptive attitude tracking control for spacecraft with unknown actuator faults. *IEEE Trans. Ind. Electron.* **2019**, *67*, 2241–2250. [CrossRef]
24. Yu, H.; Chen, X.; Chen, T.; Hao, F. Event-triggered bipartite consensus for multiagent systems: A Zeno-free analysis. *IEEE Trans. Autom. Control* **2019**, *65*, 4866–4873. [CrossRef]
25. Yu, H.; Chen, T. On Zeno behavior in event-triggered finite-time consensus of multiagent systems. *IEEE Trans. Autom. Control* **2020**, *66*, 4700–4714. [CrossRef]
26. Borgers, D.P.; Heemels, W.M.H. Event-separation properties of event-triggered control systems. *IEEE Trans. Autom. Control* **2014**, *59*, 2644–2656. [CrossRef]
27. Xing, L.; Wen, C.; Liu, Z.; Su, H.; Cai, J. Event-triggered adaptive control for a class of uncertain nonlinear systems. *IEEE Trans. Autom. Control* **2016**, *62*, 2071–2076. [CrossRef]
28. Huang, J.; Wang, Q.G. Event-triggered adaptive control of a class of nonlinear systems. *ISA Trans.* **2019**, *94*, 10–16. [CrossRef]
29. Wang, C.; Wen, C.; Hu, Q. Event-triggered adaptive control for a class of nonlinear systems with unknown control direction and sensor faults. *IEEE Trans. Autom. Control* **2020**, *65*, 763–770. [CrossRef]
30. Liang, H.; Liu, G.; Zhang, H.; Huang, T. Neural-network-based event-triggered adaptive control of nonaffine nonlinear multiagent systems with dynamic uncertainties. *IEEE Trans. Neural Netw. Learn. Syst.* **2020**, *32*, 2239–2250. [CrossRef]
31. Zhu, G.; Wang, S.; Sun, L.; Ge, W.; Zhang, X. Output feedback adaptive dynamic surface sliding-mode control for quadrotor UAVs with tracking error constraints. *Complexity* **2020**, *2020*, 8537198. [CrossRef]

32. Alexis, K.; Nikolakopoulos, G.; Tzes, A. Model predictive quadrotor control: Attitude, altitude and position experimental studies. *IET Control Theory Appl.* **2012**, *6*, 1812–1827. [CrossRef]
33. Sanner, R.M.; Slotine, J. Gaussian networks for direct adaptive control. *IEEE Trans. Neural Netw.* **1992**, *3*, 837–863. [CrossRef]
34. Zhang, X.; Wang, Y.; Zhu, G.; Chen, X.; Li, Z.; Wang, C.; Su, C.Y. Compound adaptive fuzzy quantized control for quadrotor and its experimental verification. *IEEE Trans. Cybern.* **2020**, *51*, 1121–1133. [CrossRef] [PubMed]
35. KrstiC, M.; Kanellakopoulos, I.; KokotoviC, P.V. Nonlinear design of adaptive controllers for linear systems. *IEEE Trans. Autom. Control* **1994**, *39*, 738–752. [CrossRef]
36. Esfandiari, F.; Khalil, H.K. Output feedback stabilization of fully linearizable systems. *Int. J. Control* **1992**, *56*, 1007–1037. [CrossRef]
37. Zhang, X.; Wang, Y.; Wang, C.; Su, C.Y.; Li, Z.; Chen, X. Adaptive estimated inverse output-feedback quantized control for piezoelectric positioning stage. *IEEE Trans. Cybern.* **2018**, *49*, 2106–2118. [CrossRef] [PubMed]